

Lab on a Chip

Accepted Manuscript



This is an *Accepted Manuscript*, which has been through the RSC Publishing peer review process and has been accepted for publication.

Accepted Manuscripts are published online shortly after acceptance, which is prior to technical editing, formatting and proof reading. This free service from RSC Publishing allows authors to make their results available to the community, in citable form, before publication of the edited article. This *Accepted Manuscript* will be replaced by the edited and formatted *Advance Article* as soon as this is available.

To cite this manuscript please use its permanent Digital Object Identifier (DOI®), which is identical for all formats of publication.

More information about *Accepted Manuscripts* can be found in the [Information for Authors](#).

Please note that technical editing may introduce minor changes to the text and/or graphics contained in the manuscript submitted by the author(s) which may alter content, and that the standard [Terms & Conditions](#) and the [ethical guidelines](#) that apply to the journal are still applicable. In no event shall the RSC be held responsible for any errors or omissions in these *Accepted Manuscript* manuscripts or any consequences arising from the use of any information contained in them.

ARTICLE

Continuous flow real-time PCR device using multi-channel fluorescence excitation and detection

Cite this: DOI: 10.1039/x0xx00000x

Andrew C. Hatch,^{‡,*a} Tathagata Ray,^{‡a} Kelly Lintecum,^a and Cody Youngbull^aReceived 00th January 2012,
Accepted 00th January 2012

DOI: 10.1039/x0xx00000x

www.rsc.org/

High throughput automation is greatly enhanced using techniques that employ conveyor belt strategies with un-interrupted streams of flow. We have developed a 'conveyor belt' analog for high throughput real-time quantitative Polymerase Chain Reaction (qPCR) using droplet emulsion technology. We developed a low power, portable device that employs LED and fiber optic fluorescence excitation in conjunction with a continuous flow thermal cycler to achieve multi-channel fluorescence detection for real-time fluorescence measurements. Continuously streaming fluid plugs or droplets pass through tubing wrapped around a two-temperature zone thermal block with each wrap of tubing fluorescently coupled to a 64-channel multi-anode PMT. This work demonstrates real-time qPCR of 0.1-10 μL droplets or fluid plugs over a range of 7 orders of magnitude concentration from 1×10^1 - 1×10^7 . The Real-Time qPCR analysis allows dynamic range quantification as high as 1×10^7 copies per 10 μL reaction, with PCR efficiencies within the range of 90%-110% based on serial dilution assays and a limit of detection of 10 copies/rxn. The combined functionality of continuous flow, low power thermal cycling, high throughput sample processing, and real-time qPCR improves the rates at which biological or environmental samples can be continuously sampled and analyzed.

Introduction,

Quantitative PCR is widely used for detecting and quantifying specific nucleic acid content in various fluids¹⁻⁵. The growing demands of environmental water sampling, medical diagnostics and laboratory research require greater throughputs and higher specificity, reliability, and accuracy than ever before. Often, multiple samples may need to be collected over time then analyzed immediately. Traditional PCR requires multiple heating and cooling cycles to amplify the nucleic acids, this is power intensive and time consuming. By implementing a continuous flow sample throughput design, multiple samples can be processed quickly, efficiently, and in a semi-automated fashion^{6,7}.

Many approaches have been developed to perform continuous flow PCR thermocycling, these vary in form from planar on-chip microfluidic approaches⁶⁻¹⁵ to tubing wrapped around heaters¹⁶⁻¹⁹. These devices have demonstrated amplification of nucleic acids for detection and amplification but have thus far lacked real-time quantitative capability of multiple samples¹³⁻¹⁶. A major reason for this lack of real-time quantification is due to the inability to identify discrete cycle steps through which all PCR reagents flow while migrating through the various thermal cycles^{20,21}. Using an immiscible carrier phase to isolate a PCR solution into discrete plugs or droplets makes it possible to trace exact thermal cycle for improved quantification^{7-10,17}. In addition, droplet emulsions are favorable for high throughput continuous flow processing because their liquid form enables rapid automation and simple manipulation with minimal cross-talk and sample to sample

contamination^{17,18,22-26}. Each droplet or fluid plug acts as an individual reactor to amplify as few as a single template of DNA, and each one can contain a varied library of primers and probes for detecting different template sequences^{10,26-30}.

Previous works have been able to demonstrate digital PCR quantification and real-time characterization using two-phase fluid emulsions in continuous flow devices^{6,18}. However, short of the ability to track individual plugs from start to finish they have only alluded to the ability to perform real-time quantification using scanning fluorescence observation at isolated regions. These approaches have not yet demonstrated continuous fluorescence detection of all thermal cycles simultaneously. In this work a two-phase droplet emulsion based PCR approach is used to perform continuous flow real-time qPCR analysis that tracks each discrete plug or droplet from start to finish (40 cycles) with continuous real-time fluorescence monitoring. This is accomplished using fiber optic coupling of an excitation LED source to 37 wraps of fluorinated ethylene propylene (FEP) tubing, then to a 64-channel multi-anode PMT. This work presents a PCR amplification device that can easily modify reaction volumes (0.1-10 μL), and obtain good accuracy (1.5 Ct resolution), sensitivity (10 copies/rxn) and dynamic range (7 orders of magnitude) of expected starting nucleotide concentrations. The continuous flow thermal cycling device reduces total power consumption and provides a conveyor belt like throughput for multiple analyte detection in rapid succession. A summary of the system architecture and components is provided in Figure 1.

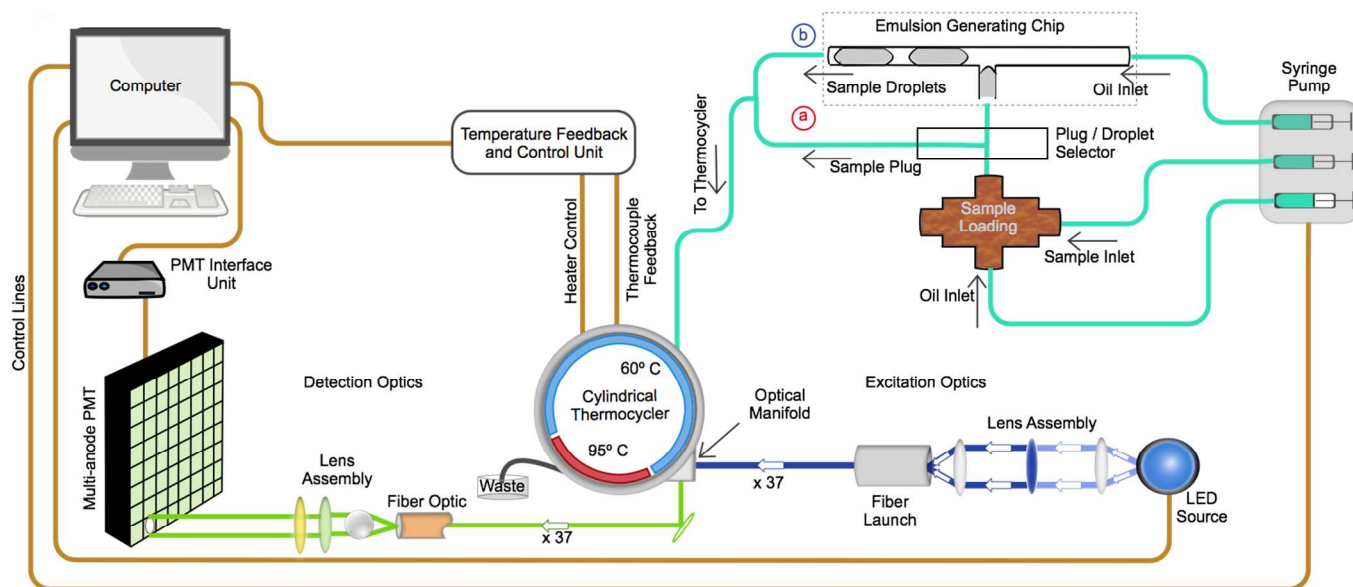


Figure 1: Overview of the system architecture of the real-time PCR instrument. Sample injection takes place through the Sample Loading device, the plug/droplet selector determines if the sample is run as a single plug (path a) or broken up into multiple droplets (path b), sample then feeds through the thermocycler while fluorescence detection is measured by the optical components.

Results and Discussion

Optical Fluorescence Detection

Characterization of the implemented fluorescence detection scheme was performed to quantify the optical coupling efficiency between the LED, tubing, and multi-anode PMT components. The optical intensity of each excitation fiber's output was measured to provide an average of $674 \pm 74 \mu\text{W}$ intensities with a min of $540 \mu\text{W}$ and a max of $800 \mu\text{W}$ yielding a coefficient of variation, CV, of 11%. For reasons mentioned in the experimental section, only 37 optical fibers were available for fluorescence excitation and were distributed to channels 1, and 5-40 with no data collected for channels 2-4. To determine optical coupling efficiency of the entire system, a reference solution of 200 nM fluorescein was passed through the tubing and measured with the optical setup with results shown in Figure 2(c). The reference solution was found to yield a mean intensity value of 9.6 ± 6.2 a.u. with a min of 1.9 a.u. and a max of 26.0 a.u. yielding a CV of 64%. All PCR reactions were normalized to these values to correct for variations in

optical coupling efficiencies of individual channels. Post normalization data had a coefficient of variation of less than 10% on average. Using the triggering mode of the PMT's Vertilon interface board, the LED was pulsed only during data capture at a rate of 30-60Hz for 2.5ms, which reduced the overall power requirement for the LED to <1 Watt. The interface board that supplied power to the PMT draws about 10 Watts.

A MATLAB® script was developed to analyze data from all 37 channels and track the droplet order from one cycle to the next. The sizes of the droplets or plugs were chosen so that they were larger than the dimensions of the tubing to preserve the droplet sequence across all cycles. To account for the possibility of coalescence and/or breakup of the fluid plugs propagating through the tubing, the detection algorithm was designed to collate the data and distinguish between different reaction numbers and volumes. After extracting the recorded average peak intensities shown in Figure 2 (b), they were normalized and the relative fluorescence intensity plotted as a function of PCR cycle as illustrated in Figures 2 (a).

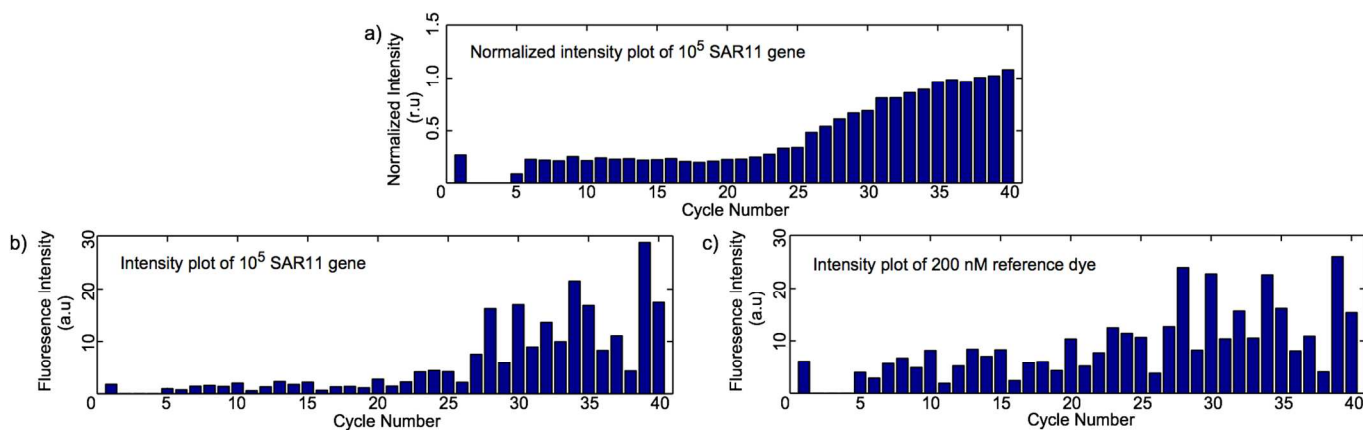


Figure 2: Real-time PCR amplification curves a) with and b) without fluorescein normalization. c) Signal output levels of 200 nm fluorescein used to normalize PCR amplification curves.

PCR Thermocycler Performance

Based on the dimensions of the thermocycler and the tubing, a single wrap around the heater was calculated to be 47 μL , yielding a total volume of 1.9 mL for the thermocycler alone. Taking into account additional lengths of tubing at the inlet and outlet, approximately 2.2 mL of oil was consumed per run. However, because of the continuous flow nature of this instrument, multiple reactions can be simultaneously run with smaller, e.g. 100 μL , volumes separating them to reduce the total amount of carrier fluid consumed per reaction. In these experiments the PCR reactions were designed for 20 seconds in the 95 $^{\circ}\text{C}$ zone and 40 seconds in the 60 $^{\circ}\text{C}$ zone. This was achieved using a fixed flow rate at 47 $\mu\text{L}/\text{min}$. Other cycle times are easily achieved using different flow rates with the ratio of 60 $^{\circ}\text{C}$ to 95 $^{\circ}\text{C}$ fixed at 2:1. Along with the flow, the temperature was closely monitored and the PID (proportional, integral, derivative) based control was able to maintain the set point temperature within 1 $^{\circ}\text{C}$. The peak power draw by the heaters during startup was limited to ~ 15 Watts for a 15 minute warm-up time, which could be reduced to < 2 minutes with higher power draws. Once the heaters equilibrated the continuous power draw was ~ 6 Watts using PWM (pulse width modulation) control. Almost 80% of the power draw resulted from a single heater at the front of 95 $^{\circ}\text{C}$ zone where the fluid transitioned from 60 $^{\circ}\text{C}$ to 95 $^{\circ}\text{C}$.

PCR Amplification

To qualify the efficiency, sensitivity, and dynamic range of the instrument, a dilution series experiment was performed on 10 μL reaction volumes of both standardized plasmid clones and environmental samples provided by the Monterey Bay Aquarium Research Institute (MBARI). Using the fluid routing scheme illustrated in Figure 1, samples could be loaded with no detectable cross-contamination between runs. The results shown in Figure 3 demonstrate a serial dilution and standard curve analysis of SAR11 reference genes in the range of NTC to 10^7 copies/rxn. For these reactions, 10- μL volumes of PCR solutions were arranged in a random sequence and aspirated in from the sample tube then pushed through the thermocycler one by one using FC40 oil as the carrier phase.

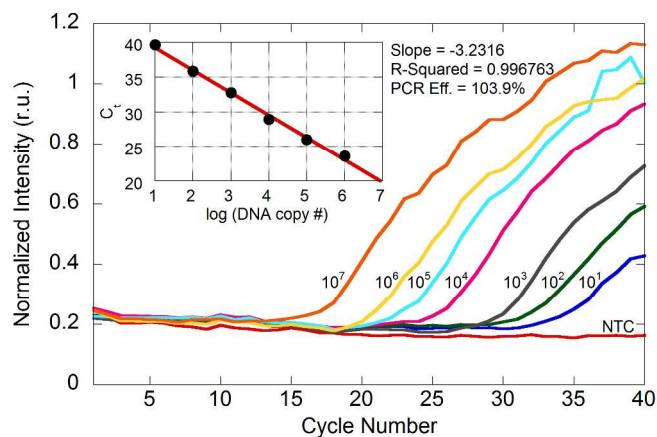


Figure 3: Serial dilution of PCR amplification with an inset of the real-time standard curve. PCR curves are plotted with a three data point moving average smoothing operation.

The cycle thresholds (Ct) for the real-time PCR reactions were determined using a threshold detection method and the PCR efficiency calculated to be 104% based on a 7-log serial dilution standard curve analysis with an R^2 value of 0.9967. Results are summarized in Table 1 with methods described in the experimental section. The acceptable range for PCR efficiencies calculated using 5-log, or greater, standard curve serial dilution experiments is 90%-110% (i.e. a slope between 3.1 and 3.58)³²⁻³⁵. A greater than 100% PCR efficiency calculation does not indicate that the PCR is performing beyond the theoretical limit, it is simply an indication that the PCR efficiency is close to optimal but the serial dilution is slightly compressed, possibly due to variations in enzyme efficiency, variations in dilution of sample inhibitors, or small pipetting errors. Since all experiments were performed in triplicate and a randomized order, any random bias from noise or user error were likely eliminated and are good indicators of the instruments reproducibility and accuracy. The limit of detection for the instrument was estimated to be 10 copies/rxn with an accuracy of 1.5 Ct. Using different reaction volumes in the range of 0.1 μL to 10 μL showed little or no change in the PCR experimental results. These performance metrics demonstrate that the PCR instrument has acceptable thermocycling and real-time fluorescence detection behavior over a large dynamic range.

One artifact of the fluorescence normalization process used to generate the curves is that the signal to background levels varied from 20:1 for the better optically coupled channels but as low as 3.3:1 for the weaker channels. This variation introduces a nonrandom bias of the instrument but since it is intrinsic to the optical fiber and PMT hardware it can be corrected through normalization. However, other sources of error resulting from electronic signal noise levels and variations in droplet sizes are random and contribute to a reduced accuracy in cycle threshold determinations.

To account for errors in pipetting accuracy, PCR volume variations, and fluorescence signal noise, commercial benchtop instruments commonly normalize their measurements with a separate color reference dye, e.g. Rox, within each PCR reaction. As designed, our system does not accommodate such an approach. The 64-channel multi-anode PMT was designed to house 40 channels for FAM fluorophore detection and 24 additional fibers of a second color for detecting a reference dye or a secondary probe fluorophore. However, due to the inability to independently control the gain of the remaining 24 channels from the first 40, they proved ineffective for measuring fluorescence and thus remained unused. The solution is to do an independent calibration run with a fluorophore at fixed concentration, the results of that run is what was used for normalization in these experiments.

Table 1: Summary of PCR dilution series runs in triplicate using SAR11 reference gene

Copies	Run 1	Run 2	Run 3	Std. Dev.	Mean
1x10 ¹	39.68	37.8	no detect	1.33	38.74
1x10 ²	35.85	36.04	35.3	0.38	35.73
1x10 ³	32.78	33.12	32.6	0.26	32.83
1x10 ⁴	28.96	29.00	28.76	0.13	28.91
1x10 ⁵	25.99	25.49	25.7	0.25	25.73
1x10 ⁶	23.61	23.35	23.18	0.22	23.38
1x10 ⁷	19.95	20.42	20.51	0.30	20.29

Experimental

Materials and methods

PCR Reagents 5' nuclease assays were performed in triplicate in a final volume of 10 μ l containing 250 nM of Taqman® hydrolysis probe (5' FAM-TTACCGCGGCTGCTGGCAC-MGB/NFQ 3'), 900 nM of forward (5'-CTCTTTCGTCGGGGAAGAAA-3') and reverse (5'-CCACCTACGWGCTCTTTAAGC-3') primer (Applied Biosystems, USA), 1x Taqman Universal PCR Mastermix (Applied Biosystems, USA), 0.175 units/ μ l of recombinant Taq DNA polymerase (Thermo Scientific, USA), and 10¹ to 10⁷ copies/rxn of plasmid DNA then brought to volume with nuclease-free (Diethylpyrocarbonate) DEPC-treated water (Ambion®, USA). Addition of the recombinant Taq DNA polymerase allowed cycling without an initial hot start recommended for the AmpliTaq® gold polymerase.

PLASMID CLONES On 4 December 2006 seawater was collected by Niskin bottle mounted on the ROV Ventana (Dive 2930) at 815 meters depth in the oxygen minimum zone (36.74407113, -122.0191486). Extraction of environmental DNA and construction of previous SAR11 rDNA clones was described previously^{36,37} with the exception that clone O2120406B10 used in this study had insert generated by PCR with Platinum® Taq DNA polymerase, was ligated into the vector pCR™4-TOPO® TA, and then was transformed into Escherichia coli One Shot TOP10 (Invitrogen, USA). Primer and probe sequences targeting the SAR11 cluster of alpha proteobacteria was described previously³⁸. Plasmids from transformed cells were purified with the QIAGEN plasmid Midi kit (Qiagen, Germany) and linearized with FastDigest Not I (Thermo Scientific, USA) according to manufacturer's directions. Agilent 2100 Bioanalyzer analysis provided by The School of Life Sciences DNA Laboratory at Arizona State University was used to confirm plasmid size and concentration before calculation of copy number.

FLUID MANIPULATION AND DROPLET GENERATION Nucleic acids were amplified using a two phase emulsion of discrete PCR volumes ranging from 100 nL droplets to as large as 10 μ l slugs. A low viscosity fluorinated oil (FC-40, 3M USA) was used as the carrier fluid and a biocompatible PFPE-PEG fluorosurfactant (FluorN 14600 Cytonix, USA) was used 0.1% concentration by weight to reduce the interfacial tension of the droplets. This also facilitates droplet break-up and reduces the likelihood of adjacent droplets coalescing while traveling through the tubing^{39-41,35}. For large volume PCR reactions, 1-10

μ l volumes of reagent were metered into a fluid routing manifold then routed into the device using the oil/surfactant carrier fluid. These could then be directly injected into the tubing of the thermocycler as shown in Figure 1 option (a). For smaller volume PCR reactions, the larger plugs could be routed through a droplet microfluidic chip to break up the slugs into smaller droplets shown in Figure 1 option (b). To verify there was no carryover from run to run, no-template-controls with nuclease-free Ambion® DEPC-treated water were run between experiments to verify there was no uptake of residual nucleic acids from previous runs.

Microfluidic devices were fabricated out of PDMS (Sylgard 184, Dow Corning) using soft lithography⁴² techniques to make droplet generating channels. The microfluidic surfaces were treated with a fluorinated ABCR silane using previously described techniques²⁹ to reduce surface interactions with the aqueous fluid phases and improve biocompatibility. Depending on the desired droplet volume, T-channel droplet generators with dimensions ranging from 100-500 μ m in width and 100-250 μ m in height were used to discretize a continuous stream of PCR reagent into a segmented oil/water droplet emulsion. Flow rates were adjusted to provide the proper volumetric throughput of 47 μ L/min through the thermocycler and their oil/PCR reagent flow rates adjusted to yield a proper shear profile for droplet breakup^{43,44}. All fluid connections on and off chip were formed using 1/16" Upchurch fitting connectors and FEP sleeves with 1/16" outer diameter (OD) and inner diameter (ID) matching the 1 mm OD of the FEP tubing wrapped around the thermocycler.

CONTINUOUS FLOW THERMOCYCLER The Continuous flow PCR thermocycler used a 10 m length of FEP tubing with 1 mm OD and 0.5 mm ID (Upchurch Scientific, USA) wrapped 40 turns around a cylindrical two-temperature aluminum thermal block. The two thermal blocks and an optical fiber coupling block were machined in aluminum and held together in a cylindrical shape using two Delrin® rings positioned top and bottom. The heater was dimensioned to a 2" height, 3" OD, 2.75" ID and a 0.5" spacing between the two pieces where the optical coupling block was positioned. The circumferential ratio of each aluminum piece was patterned to provide a 5" 60 °C arc length and 3" 95 °C arc length of tubing with a 0.5" linear distance between them to separate the temperature zones and accommodate optical fiber coupling to each wrap of tubing. Thin film low voltage resistive Kapton heaters, (Omega, USA) were attached to the inner surface of each aluminum piece and the temperature profiles were independently controlled using thermocouple feedback to a custom made temperature control board. The inner and outer surfaces of the aluminum block heater and tubing assembly were covered inside and out with cylindrically shaped 0.5" thick low density foam for insulation to equilibrate temperature profiles and reduce energy consumption.

The FEP tubing was wrapped around the thermocycler so as to pass from the 60 °C annealing and extension phase through the optical detector manifold then to the 95 °C melting phase and back to the 60 °C side as seen in Figure 4. Thermal cycling times were dependent on circumference of the thermocycler, the inner diameter of the tubing, and the volumetric fluid flow rates passing through them. Using this fixed aspect ratio geometry, the ratio of hot and cold residence times were fixed to a 2:1 ratio but the flow rates were adjusted to accommodate 30 s to 1 min cycle times. Typical PCR thermoprofiles utilize a 15s hold time at 95 °C (hot) and 60s hold time at 60 °C (cold)

with a thermal ramp time of 2-5 °C/s which equates to a 2.5:1 ratio for total cold:hot cycle time. For shortened PCR thermocycles, ramp and hold times are reduced as much as possible, disproportionately so for the 60 °C time as compared to the 95 °C time. Taken to the extreme, this ratio has been published³¹ with total cycle times as low as 5s and 60 °C:95 °C ratios of 1:1. Here, the 2:1 ratio was chosen to accommodate shortened PCR thermocycling times between 30s to 60s per cycle, allowing for a 5s thermal ramp time.

Given a 500 μm ID, a single wrap of tubing around the 3" OD heater holds 47 μL of fluid yielding a total of 1.9 mL of swept volume over the 40 wraps of tubing plus an additional 0.12 mL volume in two 12" lengths of excess tubing at the inlet and outlet. A single wrap of tubing has a length of ~240 mm with a 1 μL volume every ~5.1 mm.

To achieve a 1 minute cycle time, a flow rate of 47 μL/min was used yielding a 20 s ramp/hold time at 95 °C and a 40 s ramp/hold time at 60 °C. Empirically we measured the temperature of the tubing on both the heater side and insulation side and found a less than 2C variation. By the same approach, we estimated the time required for the temperature of the fluid to change from one zone to the next to be ~5 seconds. During operation the pressure difference from inlet to outlet was measured using an inline Honeywell pressure sensor (model no. 26PCFFA6G) and found to be 3-7 Psi depending on the number of droplets or slugs present in the line which are known to cause some feedback in the pressure⁴⁵.

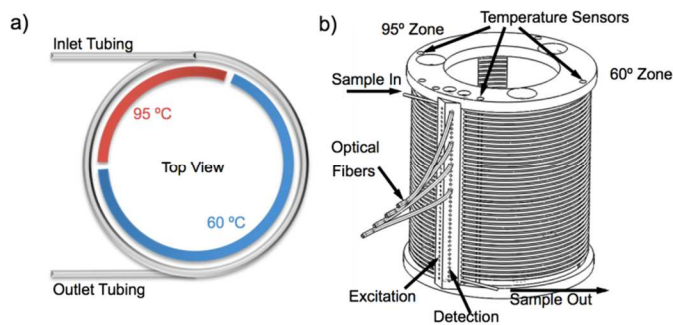


Figure 4: Schematic of the continuous flow PCR device depicting, a) the temperature profile, and b) the two zone thermocycler, tubing, temperature sensors, optical fiber coupling and inlet and outlet ports.

Multi-channel real-time fluorescence detection Real-time Fluorescence detection was accomplished using 400 μm core 0.22 NA, high-OH, silica optical fibers (Polymicro Technologies, USA) to bring an M470L2 mounted blue LED with 470 nm nominal wavelength and 950 mW output power (Thorlabs, USA) to 37 wraps of PCR tubing and couple the fluorescence emission to a photodetector. The photodetector consists of a 64-channel multi-anode PMT in an 8x8 configuration (H8500 Hamamatsu, USA) which interfaces to a Vertilon SIB064A board that communicates to a computer through a PhotonIQ IQSP482 DAQ system (Vertilon, USA). The LED excitation light source passes through an FF02-475/50-25 interference excitation filter (Semrock, USA) and a 1" ACL250 aspheric condenser lens (ThorLabs, USA) then launches into a custom fabricated close packed bundle of 37 fibers (Polymicro Technologies, USA). The output intensity of each excitation fiber was measured using an optical power meter kit (PM130D, ThorLabs).

The optical fiber bundle was custom assembled by Polymicro Technologies to house a close packed 0.5 m long fiber bundle containing 37 400-μm fibers in a 3/16" ID aluminum housing with 1/2" OD and a strain relief. The 1/2" length of the standard polyimide fiber coating was stripped away on both the inlet and outlet side using their laser etching technique. These 37 fibers were coupled to the wrapped FEP tubing on cycles 1 and 5-40 for fluorescence excitation at an angle of 30° using a custom machined fiber coupling block made of aluminum. A second set of optical fibers were coupled from the FEP tubing at a complimentary angle of 30° from normal for fluorescence emission. Optical coupling gel was used to reduce non-uniformities in optical coupling efficiencies and increase overall signal to noise ratios.

Each emission fiber was coupled to a custom fabricated optical assembly as illustrated in Figure 5. The emission output of each optical fiber was first collimated through a low cost 3 mm glass bead (Sigma-Aldrich, USA) then passed through a green (FF01 540/50 Semrock, USA) interference filter followed by a 3 mm glass absorption filter (FSQOG515 Newport, USA) before coupling to the PMT. Fluorescence detection was collected at 30-200 Hz frequencies depending on droplet size and spacing with a voltage gain setting of 400-450 V and an integration time of 2.5 ms. The blue excitation LED was synchronously pulsed on and off with the data capture times using TTL control logic from the Vertilon DAQ board to the LEDD1B Thorlabs power driver.

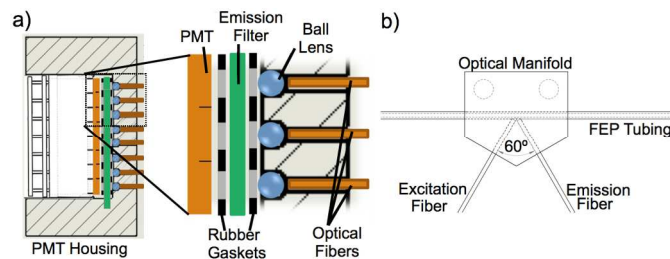


Figure 5: a) Schematic of the multichannel LED excitation block. b) Cross-section of the fiber coupling Schematic of detection block showing how the optical fibers interface with the 64-channel PMT block

As not all fibers coupled to the FEP tubing and PMT device with the same efficiency, Fluorescence signals were normalized to the intensity measurements of a standard solution of 200 nM fluorescein (Sigma Aldrich, USA) in Tris_HCl 0.1M pH 8.0 buffer solution (Fisher Scientific, USA). Droplets were tracked based on their sequential order while passing through the tubing since the ID of the tubing was the same size or smaller than the droplet diameter which prevented droplets from passing by one another. The data was processed using custom MATLAB® scripts to perform peak detection algorithms and track each droplet while passing from cycle to cycle.

Normalization was performed by subtracting the background then dividing each PCR channels fluorescence signal level by its corresponding 200 nM reference dye solutions mean intensity level. The peak intensity of each droplet was measured from cycle to cycle then the average of all droplet's relative fluorescence intensity was plotted as a function of PCR cycle. To further reduce noise levels from one channel to the next, a three point moving average smoothing operation was performed on the data. The average baseline signal levels were calculated from the first 10 valid data points and used to

interpolate the values of channels 2-5 on the PCR curves shown in Figure 3. The Ct value was then determined as the point where the fluorescence intensity rose above twice the background signal level. PCR efficiencies were calculated using the standard approach of fitting a curve to a 5-log or greater serial dilution then calculating the slope and applying it to the equation: Efficiency = $10^{(-1/\text{slope})} - 1$.

Conclusions

The continuous flow PCR instrument developed here has a great potential to be developed as a platform for performing high-throughput, real-time PCR experiments in a continuous flow manner. It can be readily modified based on the experiment's design-requirements for different sets of primers or fluorescent dyes. Simply increasing the number of tubing wraps can increase the number of cycles and changing the excitation and emission filters provides the flexibility of using other types of fluorescent dyes. The set temperature points can be easily changed based on primer probe requirements but are currently designed to be uniformly similar over all 40 cycles.

This instrument initial design is focused towards a low power instrument that can be easily transported for portable location analysis, eliminating the need for transporting samples to full-scale laboratories. A suite of experiments can be performed in less than two hours with less than 60 watt-hours of power. Any standard laptop can be used for data analysis for rapid results. Future design iterations hope to maintain system performance while yet further reducing the overall size and power demands of the system using OEM system components and simplifying data analysis routines for on the fly processing.

Acknowledgements

The work was performed on behalf of the Monterey Bay Aquarium Research Institute (MBARI) with financial support from the Gordon and Betty Moore Foundation. The authors would like to thank the excellent scientists at MBARI. We also thank Joseph Chao and Jeff Houkal for their help with mechanical design and manufacturing.

Notes and references

^a Arizona State University School of Earth and Space Exploration, 781 E Terrace Road, ISTB4 Room 795, Tempe, AZ 85287.

[†] Abbreviations: PCR, Polymerase Chain reaction, RT-PCR, Reverse Transcription PCR, qPCR, quantitative PCR, DNA, Deoxyribonucleic acids, RNA, Ribonucleic acids, Ct, cycle threshold, CV, coefficient of variation, PWM, pulse width modulation, PID, proportional integral derivative, NA, numerical aperture, a.u., arbitrary units, r.u. relative units, rxn., reaction.

[‡] These authors contributed equally.

- J. Logan, *Real-time PCR: current technology and applications*, Caister Academic Press, Norfolk UK, 2009.
- K. B. Mullis, *Ann. Biol. Clin. (Paris)*, 1990, **48**, 579–582.
- C. A. Heid, J. Stevens, K. J. Livak, and P. M. Williams, *Genome research*, 1996, **6**, 986–994.
- S. Weaver, S. Dube, A. Mir, J. Qin, G. Sun, R. Ramakrishnan, R. C. Jones, and K. J. Livak, *Methods*, 2010, **50**, 271–276.
- H. VanGuilder, K. Vrana, and W. Freeman, *Biotech.*, 2008, **44**, 619–626.
- M. M. Kiss, L. Ortoleva-Donnelly, N. R. Beer, J. Warner, C. G. Bailey, B. W. Colston, J. M. Rothberg, D. R. Link, and J. H. Leamon, *Analytical Chemistry*, 2008, **80**, 8975–8981.
- M. Chabert, K. D. Dorfman, P. de Cremoux, J. Roeraade, and J.-L. Viovy, *Analytical Chemistry*, 2006, **78**, 7722–7728.
- P. J. Obeid, T. K. Christopoulos, H. J. Crabtree, and C. J. Backhouse, *Anal. Chem.*, 2002, **75**, 288–295.
- J. Felbel, A. Reichert, M. Kielpinski, M. Urban, N. Häfner, M. Dürst, J. M. Köhler, J. Weber, and T. Henkel, *Engineering in Life Sciences*, 2008, **8**, 68–72.
- Y. Schaerli, R. C. Wootton, T. Robinson, V. Stein, C. Dunsby, M. A. Neil, P. M. French, A. J. Demello, C. Abell, and F. Hollfelder, *Analytical Chemistry*, 2009, **81**, 302–306.
- S. O. Sundberg, C. T. Wittwer, C. Gao, and B. K. Gale, *Analytical Chemistry*, 2010, **82**, 1546–1550.
- S. Mohr, Y.-H. Zhang, A. Macaskill, P. J. R. Day, R. W. Barber, N. J. Goddard, D. R. Emerson, and P. R. Fielden, *Microfluidics and Nanofluidics*, 2007, **3**, 611–621.
- M. Hashimoto, P.-C. Chen, M. W. Mitchell, D. E. Nikitopoulos, S. A. Soper, and M. C. Murphy, *Lab Chip*, 2004, **4**, 638–645.
- M. U. Kopp, A. J. de Mello, and A. Manz, *Science*, 1998, **280**, 1046–1048.
- N. Crews, C. Wittwer, and B. Gale, *Biomedical Microdevices*, 2007, **10**, 187–195.
- N. Park, S. Kim, and J. H. Hahn, *Anal. Chem.*, 2003, **75**, 6029–6033.
- M. Curcio and J. Roeraade, *Anal. Chem.*, 2002, **75**, 1–7.
- K. D. Dorfman, M. Chabert, J.-H. Codarbox, G. Rousseau, P. de Cremoux, and J.-L. Viovy, *Anal. Chem.*, 2005, **77**, 3700–3704.
- A. L. Markey, S. Mohr, and P. J. R. Day, *Methods*, 2010, **50**, 277–281.
- R. Higuchi, C. Fockler, G. Dollinger, and R. Watson, *Nat Biotech*, 1993, **11**, 1026–1030.
- S. Wang and W. Wang, *Sci. China Technol. Sci.*, 2010, **53**, 1967–1972.
- X. Niu, M. Zhang, S. Peng, W. Wen, and P. Sheng, *Biomicrofluidics*, 2007, **1**, 44101.
- Y. Schaerli and F. Hollfelder, *Mol Biosyst*, 2009, **5**, 1392–1404.
- B. T. Kelly, J.-C. Baret, V. Taly, and A. D. Griffiths, *Chemical Communications (Cambridge, England)*, 2007, 1773–1788.
- A. Huebner, S. Sharma, M. Srisa-Art, F. Hollfelder, J. B. Edel, and A. J. deMello, *Lab on a Chip*, 2008, **8**, 1244–1254.
- A. D. Griffiths and D. S. Tawfik, *Trends Biotechnol*, 2006, **24**, 395–402.
- Q. Zhong, S. Bhattacharya, S. Kotsopoulos, J. Olson, V. Taly, A. D. Griffiths, D. R. Link, and J. W. Larson, *Lab Chip*, 2011, **11**, 2167–2174.
- V. Trivedi, A. Doshi, G. K. Kurup, E. Ereifej, P. J. Vandevord, and A. S. Basu, *Lab Chip*, 2010, **10**, 2433–2442.
- A. B. Theberge, E. Mayot, A. El Harrak, F. Kleinschmidt, W. T. S. Huck, and A. D. Griffiths, *Lab Chip*, 2012, **12**, 1320–1326.
- N. R. Beer, E. K. Wheeler, L. Lee-Houghton, N. Watkins, S. Nasarabadi, N. Hebert, P. Leung, D. W. Arnold, C. G. Bailey, and B. W. Colston, *Analytical Chemistry*, 2008, **80**, 1854–1858.
- E. K. Wheeler, C. A. Hara, J. Frank, J. Deotte, S. B. Hall, W. Benett, C. Spadaccini, and N. R. Beer, *Analyst*, 2011, **136**, 3707–3712.

32. J. S. Morey, J. C. Ryan, and F. M. Dolah, *Biological Procedures Online*, 2006, **8**, 175–193.
33. M. W. Pfaffl, *AZ of quantitative PCR*, 2004, **1**, 89–113.
34. M. Kubista, J. M. Andrade, M. Bengtsson, A. Forootan, J. Jonák, K. Lind, R. Sindelka, R. Sjöback, B. Sjögreen, L. Strömbom, A. Ståhlberg, and N. Zoric, *Molecular Aspects of Medicine*, 2006, **27**, 95–125.
35. Amplification efficiency of TaqMan® Gene Expression Assays: Application Note: Life Technologies.
36. R. Massana, A. E. Murray, C. M. Preston, and E. F. DeLong, *Applied and Environmental Microbiology*, 1997, **63**, 50–56.
37. M. T. Suzuki, L. T. Taylor, and E. F. DeLong, *Applied and Environmental Microbiology*, 2000, **66**, 4605–4614.
38. M. Suzuki, C. Preston, F. Chavez, and E. DeLong, *Aquatic Microbial Ecology*, 2001, **24**, 117–127.
39. C. Holtz, A. C. Rowat, J. J. Agresti, J. B. Hutchison, F. E. Angile, C. H. J. Schmitz, S. Koster, H. Duan, K. J. Humphry, R. A. Scanga, J. S. Johnson, D. Pisignano, and D. A. Weitz, *Lab Chip*, 2008, **8**, 1632–1639.
40. D. J. Holt, R. J. Payne, W. Y. Chow, and C. Abell, *Journal of Colloid and Interface Science*, 2010, **350**, 205–211.
41. A. V. Yazdi, C. Lepilleur, E. J. Singley, W. Liu, F. A. Adamsky, R. M. Enick, and E. J. Beckman, *Fluid Phase Equilibria*, 1996, **117**, 297–303.
42. Y. Xia and G. M. Whitesides, *Annual Review of Materials Science*, 1998, **28**, 153–184.
43. V. Cristini and Y.-C. Tan, *Lab Chip*, 2004, **4**, 257–264.
44. Y.-C. Tan, V. Cristini, and A. P. Lee, *Sensors and Actuators B: Chemical*, 2006, **114**, 350–356.
45. B. J. Adzima and S. S. Velankar, *Journal of Micromechanics and Microengineering*, 2006, **16**, 1504–1510.